Spectral manifestation of optical Tamm states in a metal-cholesteric liquid crystals stack

V. Yu. Reshetnyak [1,2] I. P. Pinkevych [1] T. J. Bunning,[3] M. E. McConney,[3] and D. R. Evans [3]

[1]*Physics Faculty, Taras Shevchenko National University of Kyiv, 64 Volodymyrs'ka Street, Kyiv 01601, Ukraine*
[2]*School of Physics and Astronomy, University of Leeds, Leeds LS2 9JT, United Kingdom*
[3]*Air Force Research Laboratory, Materials and Manufacturing Directorate, Wright-Patterson Air Force Base, Dayton 45433, USA*

The reflection spectrum of linearly polarized light by a system consisting of a metal film and two adjacent sequentially located cholesteric liquid crystals (CLCs) with opposite helical twists is theoretically studied. The system contains a dielectric index-matching layer (DIML) between the metal film and the CLC layers. It is shown that in such a system the excitation of optical Tamm states (OTSs) by linearly polarized light is possible. The influence of the CLC pitch, refractive indices, and thicknesses of the DIML and metal film on the OTS manifestation in the reflection spectrum of the system is studied. The strong influence of the DIML thickness on the OTS wavelength and the appearance of multiple OTSs with an increase in the DIML thickness is noted.

I. INTRODUCTION

Significant progress has been made in the last decade in the study of localized optical states appearing near the interface between two media. In these media, electromagnetic waves decay with distance from the interface when at least one of them is a photonic crystal with the properties of a Bragg mirror. Such states are optically manifested in the form of narrow resonance peaks in reflection and transmission in the spectral range of the photonic band gap.

When adjacent media are two photonic crystals with overlapping band gaps, the localized states are called optical Tamm states (OTSs) [1–3] by analogy with Tamm surface electronic states. Localized states formed at the metal-photonic crystal interface are usually called Tamm plasmons or Tamm plasmon polaritons [4–11], since they are associated with the excitation of plasmons in the metal, but should not be confused with surface waves [5,12]. OTSs have potential use in sensors [13–17], Tamm plasmon based lasers [18–20], optical switches and filters [21–23], and selective thermal and light emitters [24–26].

Liquid crystals are known for their possible applications of controlling surface waves: surface plasmons, localized surface plasmons, and Dyakonov surface waves [27–35]. More specifically, cholesteric liquid crystals (CLCs) have properties that allow them to be used as photonic crystals: circularly polarized light incident along the CLC helical axis undergoes a Bragg reflection if the circular polarization of light coincides with the CLC helix, while light with the opposite circular polarization does not experience a Bragg reflection [36]. This makes it possible to use CLCs as Bragg mirrors in structures for exciting and studying OTSs. In particular, as shown in Ref [37], if a quarter-wave-length anisotropic film is placed between the CLC and the metal layer, which affects the polarization of light, OTSs can be excited in this system by circular polarized light. Exciting of OTSs by circularly

polarized light was also studied in a system consisting of the metal film adjacent to two identical CLCs with opposite helix twists [38]. In this past study, the CLCs studied were not thick and therefore allowed circularly polarized light to not be completely reflected, thereby providing only partial localization of light required to excite OTSs. Transmission peaks of circularly polarized light were obtained, corresponding to the appearance of several OTSs in such a system. The appearance of several OTSs at the interface with a metal was also demonstrated in structures with a multilayer Bragg mirror [39–41].

In this paper, the appearance of OTSs in a system consisting of a metal film and two CLC layers with opposite directions of the helix twist is considered in the field of an incident linearly polarized light wave. There is a dielectric index matching layer (DIML) near the CLCs, and, in distinction to Ref. [38], both CLCs are thick enough to provide a full reflection of waves with circular polarization coinciding with the CLC helix. It is shown that in such a system the excitation of OTSs by linearly polarized light is possible. The influence of the CLC pitch, refractive indices, and thicknesses of the DIML and the metal film on the OTS manifestation in the reflection spectrum of the system is studied.

The structure investigated in this paper is quite manageable practically. In particular, by influencing the pitch of the cholesteric helix with the help of an external field, one can shift the stop band of the system and the spectral location of the reflection dip. The same can be done by changing the thickness and/or the refractive index of the DIML between the first CLC and the metal.

The paper is organized as follows. Section II introduces a model of the system under consideration and derives equations allowing for the calculation of reflectance in the CLC band gap. Results of numerical calculations for a system with an Ag film and their discussion are presented in Sec. III. Section IV presents some conclusions.
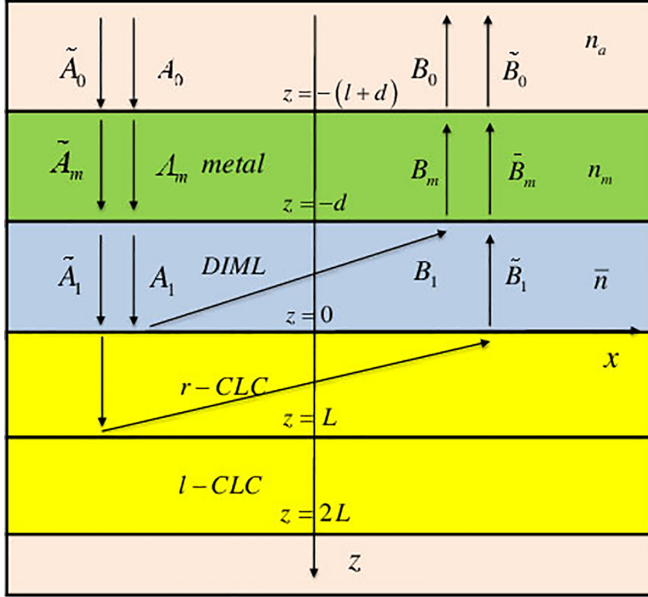
FIG. 1. Schematic of the structure "metal film-DIML-CLC layers" together with directions of the light beams propagating in the system. Letters A and B denote complex amplitudes of waves with right-handed circular polarization, while letters $\tilde{A}$ and $\tilde{B}$ (with tilde) denote complex amplitudes of waves with left-handed circular polarization; $r-CLC$ and $l-CLC$ denote CLC with right-handed and left-handed helical twists, respectively. Slanted lines indicate waves reflected from the CLC with the same helical twist as a circular polarization of incident wave; they are directed away from the corresponding incident wave arrow and are therefore inclined in the figure. n_a, n_m, and $\bar{n}$ are the refractive indices defined in the text of the paper.

II. THEORETICAL MODEL AND BASIC EQUATIONS

Suppose we have a structure consisting of a metal film on top of two planar CLCs arranged in series one after the other with opposite twists (right-handed and left-handed) of the cholesteric helix. There is also a DIML between the metal film and the first CLC layer, which affects the phase of the propagating waves and therefore the conditions for their interference near the metal film (see Fig. 1). To minimize the usual reflection of light due to the difference in the refractive indices, the DIML refractive index is taken to be equal to the average refractive index of the CLC layers. In addition, we consider only the case when the CLC layers' thickness is large enough to ensure complete reflection of the light wave with the same circular polarization as the CLC helical twist. To simplify the calculations, we will also neglect the energy dissipation in the CLC (the role of the CLC dissipation was studied, for example, in [42]).

Let the Cartesian z axis be directed along the axis of the cholesteric helices, and a plane polarized light wave be incident on the metal film along this axis. We assume that the incident wave is polarized along the x axis, and the CLC director at both boundaries of both CLC layers is also oriented along the x axis.

It is convenient to present an incident linearly polarized wave as a superposition of the right-handed and left-handed

circularly polarized waves. Then, denoting $k_0 = \omega / c$, where ω is the light wave frequency, we can present the electromagnetic wave incident on the metal film (from the top of the structure) as follows:

$$\boldsymbol{E}_{0i}(z, t) = \boldsymbol{E}_{0i}(z)e^{i\omega t},$$
$$\boldsymbol{E}_{0i}(z) = \frac{A_0}{\sqrt{2}}\binom{1}{i}e^{-ik_0 n_a z} + \frac{\tilde{A}_0}{\sqrt{2}}\binom{1}{-i}e^{-ik_0 n_a z}, \quad (1)$$

where n_a is a refractive index of the medium above the metal film, and $\binom{1}{\pm i} = \boldsymbol{e}_x \pm i\boldsymbol{e}_y$, where $\boldsymbol{e}_x$ and $\boldsymbol{e}_y$ are the unit Cartesian vectors. In Eq. (1) the terms $\frac{A_0}{\sqrt{2}}\binom{1}{i}e^{-ik_0 n_a z}$ and $\frac{\tilde{A}_0}{\sqrt{2}}\binom{1}{-i}e^{-ik_0 n_a z}$ describe the right-handed and left-handed circularly polarized waves propagating in the $+z$ direction, respectively; since the incident wave is linearly polarized along the x axis, $\tilde{A}_0 = A_0$.

The incident wave penetrates the structure shown in Fig. 1, and is reflected from the elements of this structure. The incident right-handed and left-handed circularly polarized waves can be reflected differently from the various structural elements of the system; therefore, in the general case we must seek the reflected light field in the form of a superposition of both right-handed and left-handed circularly polarized waves with different complex amplitudes. In particular, for the reflected wave above the metal film, we have

$$\boldsymbol{E}_{0r}(z) = \frac{B_0}{\sqrt{2}}\binom{1}{-i}e^{ik_0 n_a z} + \frac{\tilde{B}_0}{\sqrt{2}}\binom{1}{i}e^{ik_0 n_a z}. \quad (2)$$

The reflected waves propagate in the $-z$ direction such that in Eq. (2) the first term describes the right-handed circularly polarized wave and the second term describes the left-handed circularly polarized wave.

Similarly, in the metal film, we can present the light field as a superposition of the fields propagating in the $+z$ and $-z$ directions ($\boldsymbol{E}_{mi}$ and $\boldsymbol{E}_{mr}$, respectively), each of which is a superposition of the right and left circularly polarized waves:

$$\boldsymbol{E}_{mi} = \frac{A_m}{\sqrt{2}}\binom{1}{i}e^{-ik_0 n_m z} + \frac{\tilde{A}_m}{\sqrt{2}}\binom{1}{-i}e^{-ik_0 n_m z}, \quad (3)$$

$$\boldsymbol{E}_{mr} = \frac{B_m}{\sqrt{2}}\binom{1}{-i}e^{ik_0 n_m z} + \frac{\tilde{B}_m}{\sqrt{2}}\binom{1}{i}e^{ik_0 n_m z}, \quad (4)$$

where n_m is a complex refractive index of the metal.

In the DIML, there is an electromagnetic field propagating in the $+z$ direction and consisting of the right and left circularly polarized waves,

$$\boldsymbol{E}_{1i}(z) = \frac{A_1}{\sqrt{2}}\binom{1}{i}e^{-ik_0 \bar{n} z} + \frac{\tilde{A}_1}{\sqrt{2}}\binom{1}{-i}e^{-ik_0 \bar{n} z}, \quad (5)$$

and an electromagnetic field comprising both right and left circularly polarized waves propagating in the $-z$ direction due to reflection from the both CLC layers [43],

$$\boldsymbol{E}_{1r} = \frac{B_1}{\sqrt{2}}\binom{1}{-i}e^{ik_0 \bar{n} z} + \frac{\tilde{B}_1}{\sqrt{2}}\binom{1}{i}e^{ik_0 \bar{n} z}, \quad (6)$$

where the $\bar{n} = \sqrt{(\varepsilon_\perp + \varepsilon_\parallel)/2}$ is the DIML refractive index equal to the average refractive index of the CLC, and $\varepsilon_\perp$ and

$\varepsilon_\parallel$ are the dielectric constants of the CLC for light polarized perpendicular and parallel to the CLC director, respectively.

To be more specific, suppose that the first CLC adjacent to the DIML has the right-handed twist of the cholesteric helix, and the second CLC layer (see Fig. 1) has the left-handed twist. Since the refractive index of the DIML is equal to the average refractive index of the two CLC layers, we can neglect the usual reflection of light at the interface between the CLC layer and the DIML.

The electromagnetic field (5) transverses the DIML to the CLC layer with the right-handed twist. The right circularly polarized part of the electromagnetic field (5), $\frac{A_1}{\sqrt{2}}\binom{1}{i}e^{-ik_0\bar{n}z}$, is then reflected from the right-handed CLC in the $-z$ direction to the DIML as a right circularly polarized electromagnetic wave $\frac{B_1}{\sqrt{2}}\binom{1}{-i}e^{ik_0\bar{n}z}$ presented in Eq. (6). Therefore, according to [44,45], the amplitudes of a circularly polarized wave incident on a CLC with same handed-helical twist and subsequently reflected from that CLC layer, are connected by the relationship

$$B_1 = R_a A_1, \tag{7}$$

where R_a is an amplitude coefficient of diffraction reflection from the CLC in band gap.

The left circularly polarized part of the field (5), $\frac{\tilde{A}_1}{\sqrt{2}}\binom{1}{-i}e^{-ik_0\bar{n}z}$, passes through the right-handed CLC and reflects from the subsequent left-handed CLC resulting in a left circularly polarized wave in the $-z$ direction. This wave traveling in the $-z$ direction is unaffected by the right-handed CLC and results in a left circularly polarized field, $\frac{\tilde{B}_1}{\sqrt{2}}\binom{1}{i}e^{ik_0\bar{n}z}$, in the DIML [presented in Eq. (6)]. Taking into account that the CLC thickness is equal to an integer number of the CLC pitch, at the DIML boundary there is a relationship between the amplitudes $\tilde{A}_1$ and $\tilde{B}_1$, similar to Eq. (7):

$$\tilde{B}_1 = R_a \tilde{A}_1. \tag{8}$$

Using the results presented in [44], one can obtain the following expression for R_a:

$$R_a = \frac{i(w^2+1)(1-e^{-i2k_0n_2L})}{2w(1+e^{-i2k_0n_2L})+(w^2-1)(1-e^{-i2k_0n_2L})}, \tag{9}$$

where

$$w = \frac{ip}{2\lambda n_2}\left[n_e^2 - n_2^2 - (\lambda/p)^2\right], \tag{10}$$

$$n_2 = \pm\left[\bar{\varepsilon} + (\lambda/p)^2 - \sqrt{4\bar{\varepsilon}(\lambda/p)^2 + \delta^2}\right]^{1/2}, \tag{11}$$

$$\delta = (\varepsilon_\parallel - \varepsilon_\perp)/2, \quad \bar{\varepsilon} = (\varepsilon_\parallel + \varepsilon_\perp)/2. \tag{12}$$

In Eqs. (9)–(11), L is a CLC thickness, p is the CLC pitch, λ is a wavelength in a vacuum, n_2 takes an imaginary value in the CLC band gap, and the ratio L/p is an integer.

There is very little transmission of a normally incident circularly polarized plane wave through a CLC that has the same handedness as the incident plane wave, provided that the CLC has a sufficient number of periods and the free-space wavelength of the incident plane wave lies in the circular Bragg regime [36,45]. The incident plane wave in Eq. (1) is linearly polarized, that is, it is an equal superposition of left and right circularly polarized plane waves. Therefore, only

one circularly polarized component of the incident plane wave is reflected from the first CLC, namely of the same handedness as the CLC, and the circularly polarized component with the opposite handedness passes through this first CLC, falls on the second CLC, and is reflected from it [43]. Therefore, it is enough to consider the boundary conditions for electromagnetic field at $z = -(l+d)$ and $z = -d$, where l and d are the thicknesses of the metal film and the DIML, respectively. Using Eqs. (1)–(6) and the equation for a magnetic field, $\boldsymbol{H} = \frac{1}{i\omega\mu_0}(\boldsymbol{e}_x\frac{\partial}{\partial z}E_y - \boldsymbol{e}_y\frac{\partial}{\partial z}E_x)$, we obtain the following equations at the boundary $z = -(l+d)$:

$$2A_0 e^{ik_0 n_a(l+d)} + (B_0 + \tilde{B}_0)e^{-ik_0 n_a(l+d)}$$
$$= (A_m + \tilde{A}_m)e^{ik_0 n_m(l+d)} + (B_m + \tilde{B}_m)e^{-ik_0 n_m(l+d)},$$

$$(B_0 - \tilde{B}_0)e^{-ik_0 n_a(l+d)}$$
$$= -(A_m - \tilde{A}_m)e^{ik_0 n_m(l+d)} + (B_m - \tilde{B}_m)e^{-ik_0 n_m(l+d)}, \tag{13}$$

$$2A_0 e^{ik_0 n_a(l+d)} - (B_0 + \tilde{B}_0)e^{-ik_0 n_a(l+d)}$$
$$= \frac{n_m}{n_a}[(A_m + \tilde{A}_m)e^{ik_0 n_m(l+d)} - (B_m + \tilde{B}_m)e^{-ik_0 n_m(l+d)}],$$

$$(B_0 - \tilde{B}_0)e^{-ik_0 n_a(l+d)}$$
$$= \frac{n_m}{n_a}[(A_m - \tilde{A}_m)e^{ik_0 n_m(l+d)} + (B_m - \tilde{B}_m)e^{-ik_0 n_m(l+d)}].$$

For the boundary $z = -d$ the equations are as follows:

$$(A_m + \tilde{A}_m)e^{ik_0 n_m d} + (B_m + \tilde{B}_m)e^{-ik_0 n_m d}$$
$$= (A_1 + \tilde{A}_1)e^{ik_0 \bar{n}d} + (B_1 + \tilde{B}_1)e^{-ik_0 \bar{n}d},$$

$$(A_m - \tilde{A}_m)e^{ik_0 n_m d} - (B_m - \tilde{B}_m)e^{-ik_0 n_m d}$$
$$= (A_1 - \tilde{A}_1)e^{ik_0 \bar{n}d} - (B_1 - \tilde{B}_1)e^{-ik_0 \bar{n}d}, \tag{14}$$

$$\frac{n_m}{\bar{n}}[(A_m + \tilde{A}_m)e^{ik_0 n_m d} - (B_m + \tilde{B}_m)e^{-ik_0 n_m d}]$$
$$= (A_1 + \tilde{A}_1)e^{ik_0 \bar{n}d} - (B_1 + \tilde{B}_1)e^{-ik_0 \bar{n}d},$$

$$\frac{n_m}{\bar{n}}[(A_m - \tilde{A}_m)e^{ik_0 n_m d} + (B_m - \tilde{B}_m)e^{-ik_0 n_m d}]$$
$$= (A_1 - \tilde{A}_1)e^{ik_0 \bar{n}d} + (B_1 - \tilde{B}_1)e^{-ik_0 \bar{n}d}.$$

Substituting Eqs. (7) and (8) into Eqs. (13) and (14), one can obtain a system of equations for the amplitudes B_0 and $\tilde{B}_0$. This system has a nontrivial solution only if $B_0 = \tilde{B}_0$ and, therefore, the light reflected from the structure under consideration is linearly polarized.

Finally, the reflection coefficient of the incident linearly polarized wave from the system under consideration, $R = |B_0/A_0|^2$, is as follows:

$$R = \left|\frac{r_a(1 - rR_a e^{-i2k_0\bar{n}d}) - (r - R_a e^{-i2k_0\bar{n}d})e^{-i2k_0 n_m l}}{(1 - rR_a e^{-i2k_0\bar{n}d}) - r_a(r - R_a e^{-i2k_0\bar{n}d})e^{-i2k_0 n_m l}}\right|^2, \tag{15}$$

where

$$r = \left(1 - \frac{n_m}{\bar{n}}\right)\bigg/\left(1 + \frac{n_m}{\bar{n}}\right), \quad r_a = \left(1 - \frac{n_m}{n_a}\right)\bigg/\left(1 + \frac{n_m}{n_a}\right). \tag{16}$$

(a)

(b)
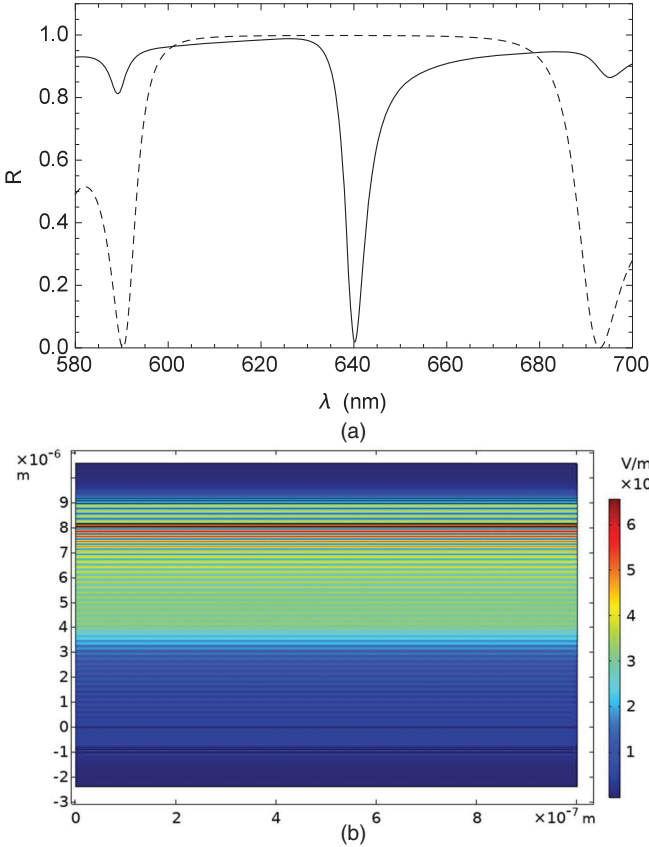
FIG. 2. (a) Reflection dip (solid line) in the spectral region of the CLC band gap (dashed line). CLC pitch $p = 400$ nm, thickness of the DIML $d = 0.3p$, thickness of the Ag film $l = 36$ nm. (b) Spatial profile of the amplitude of the electric component of the electromagnetic field at the OTS wavelength.

III. RESULTS AND DISCUSSION

The reflection spectrum of the system over the range of the CLC band gap is calculated by considering a Ag layer as a metal film on top of the structure. For the calculations, we set the refractive index of the medium above the Ag film to be $n_a = 1$, and the refractive indices of the CLC, n_o, n_e, are $n_o = 1.5$, $n_e = 1.7$ or changed by ± 0.1. The frequency dispersion of the complex refractive index of Ag is described by the expression $n_m = 0.14 + i(0.738 \times 10^7\lambda - 0.869)$ [46]. The CLC pitch p, thickness of the DIML d_1, and thickness of the Ag film l are variable parameters. The calculations show that for a CLC thickness $L \geqslant 10p$, there is no dependence of the reflection spectra on the CLC layer thickness, therefore, under this condition, the CLC can be considered thick in accordance with the requirement of our system.

Figure 2(a) shows a reflection dip in the spectral region of the CLC band gap, which is associated with the appearance of an OTS in the system shown in Fig. 1. As an example, we took the case when the CLC band gap is in the central part of the visible spectrum. In Fig. 2(b), we present the spatial profile of the amplitude of the electric component of the electromagnetic field on the OTS wavelength, which is calculated using COMSOL software for the CLC pitch $p = 400$ nm. Excitation

(a)

(b)
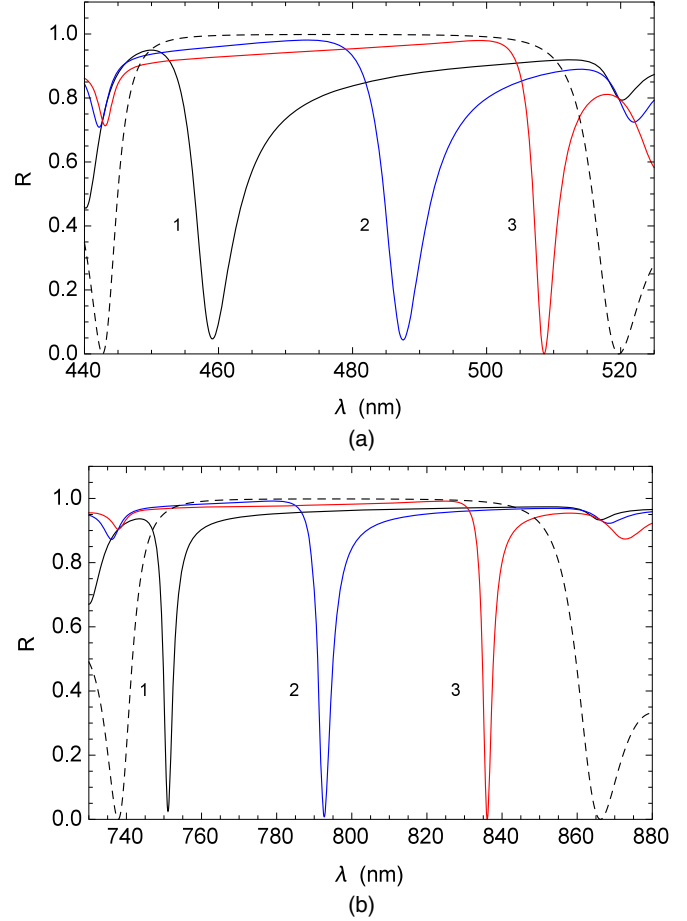
FIG. 3. Influence of the DIML thickness on the OTS spectral distribution in the CLC band gap: (a) $p = 300$ nm; (b) $p = 500$ nm; $d/p = 0.2$: 1; 0.3: 2; 0.4: 3; $l = 36$ nm. Dashed lines show the band gap.

of OTSs is evident in Fig. 2(b) as the high magnitude of the electric field near the edge of the Ag film at the OTS wavelength of 640 nm [≈ 8 μm in Fig. 2(b)].

In Fig. 3 we show the dependence of the OTS reflection dip on the thickness of the DIML, d, using CLC with two different pitches, $p = 300$ nm [Fig. 3(a)] and $p = 500$ nm [Fig. 3(b)]. One can see that the spectral position of the OTS reflection dip in the CLC band gap depends strongly on the thickness of the DIML, while the magnitude and width of the dip depends on its spectral position.

To clarify the role of the DIML it is necessary to take into account that the OTS arises due to the interference of forward and backward waves repeatedly reflected from the CLC and the metal film. The DIML, located between the Ag film and the CLC layer, affects the phase difference of these waves and, consequently, the conditions for their constructive interference, therefore the wavelength, magnitude, and width of the localized wave packet corresponding to the OTS can vary with the DIML thickness, which is observed in Fig. 3. The difference in the incursion of the phases of the forward and backward waves caused by a DIML of thickness d is $\varphi = 2\pi \frac{2d}{\lambda}\bar{n}$. For a fixed φ corresponding to an interference maximum at a wavelength λ, which can be associated with an OTS at that wavelength, an increase in d leads to an increase
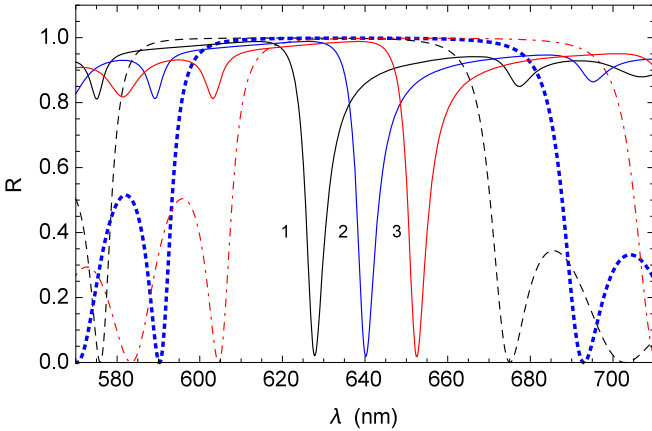
FIG. 4. Influence of the CLC pitch value on the OTS spectral position: $p(nm) = 390$: 1; 400: 2; 410: 3; $d = 120$ nm, $l = 36$ nm, $L = 4100$ nm.

of the OTS wavelength as shown in Fig. 3. In addition, since a change in the DIML thickness by $\Delta d = \frac{\lambda}{2\bar{n}}$ leads to a shift of φ by 2π, the appearance of the OTS at a given wavelength will be periodic, which is confirmed by our numerical calculations and was also noted in [38] for a system with a multilayer Bragg mirror.

Figure 4 shows the influence of the CLC pitch value on the OTS dip wavelength for a fixed DIML thickness. From Fig. 4 we can see that the wavelength of the dip increases with an increase in the helix pitch, it shifts towards a longer wavelength in accordance with the shift of the CLC reflection band.

In Fig. 5 we present results of calculations of the reflectance of the system for different thickness of the Ag film and two values of the CLC pitch ($p = 300$ nm, $p = 400$ nm), when the thickness of DIML is fixed at $d = 0.3p$. From Fig. 5 it is seen that there is an optimal thickness of the Ag film, corresponding to the maximum value of the OTS dip, $l = 40$ nm for both cases, $p = 300$ nm and $p = 400$ nm. However, the influence of the Ag film thickness on the OTS spectral position is not strong in contrast to the system without the DIML studied in [38].

An influence of the CLC refractive indices n_o and n_e on the spectral position of the OTS dip in the CLC band gap is shown in Fig. 6, which considers a CLC with the helical pitch $p = 400$ nm and a DIML thickness $d = 0.3p$. Values n_o and n_e are chosen such that the CLC band gaps are within the visible region (560–700 nm). In Fig. 6, comparing the spectral position of the OTS dips and a location of the CLC band gaps, we can see that the spectral position of the OTS dip tracks the shift of the center of the CLC band gap.

We would like to note that for the above calculations, we used relatively small thicknesses of the DIML, which are tenths of the CLC pitch. If we take large values of the DIML thickness, we can observe two and more spectral dips in the same CLC band gap. As an example, in Fig. 7 we show cases with two and three OTS dips by setting the DIML thicknesses to $d = 4.6p$ and $d = 8.3p$ with $p = 400$ nm [Figs. 7(a) and 7(b), respectively].

(a)

(b)
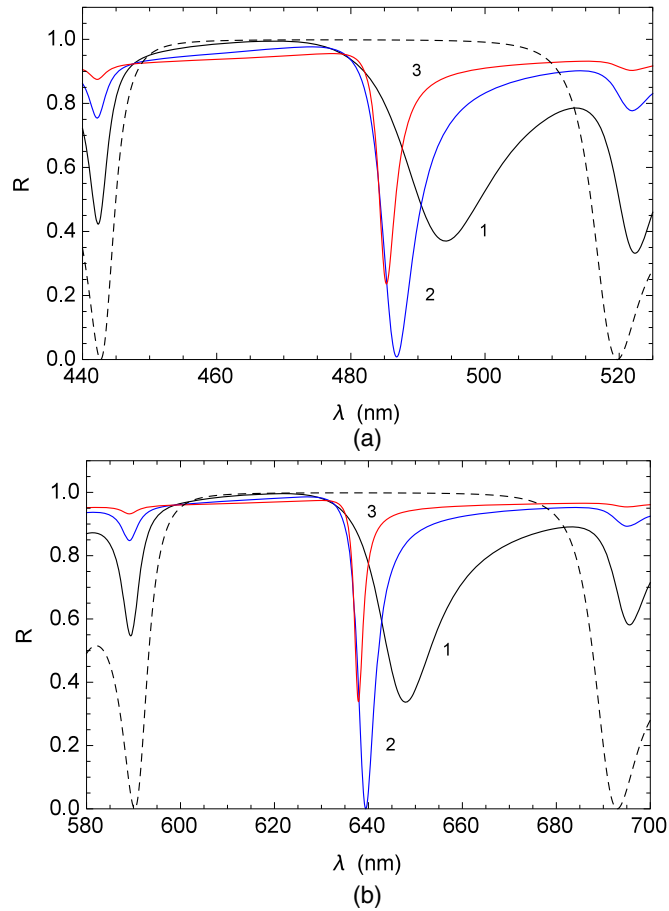
FIG. 5. Magnitude of the OTS spectral dip in the CLC reflection band at different values of the Ag film thickness: l (nm) = 20: 1; 40: 2; 60: 3; (a) $p = 300$ nm; (b) $p = 400$ nm, $d/p = 0.3$.

The relatively large DIML thickness required for the appearance of two or more OTSs in the CLC band gap can be explained if the following is taken into account. Let φ
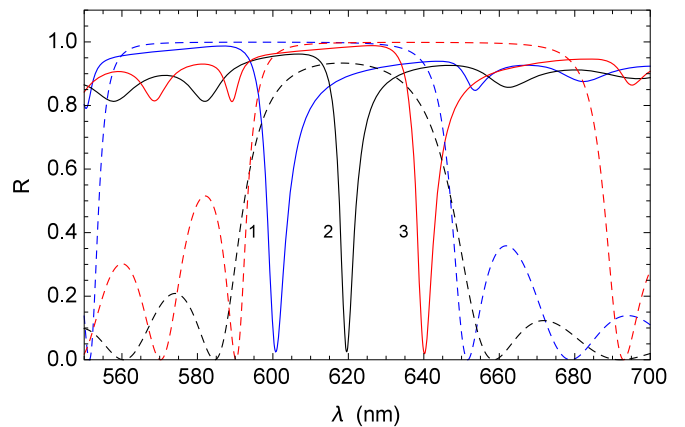
FIG. 6. Influence of the CLC refractive indices n_e and n_o on the spectral position of the OTS dip in the CLC band gap; ($n_o = 1.4$, $n_e = 1.6$): 1; ($n_o = 1.5$, $n_e = 1.6$): 2; ($n_o = 1.5$, $n_e = 1.7$): 3; $p = 400$ nm; $d/p = 0.3$, $l = 36$ nm. Dashed lines of the corresponding color show the band gaps for CLC using the same values of n_o and n_e.
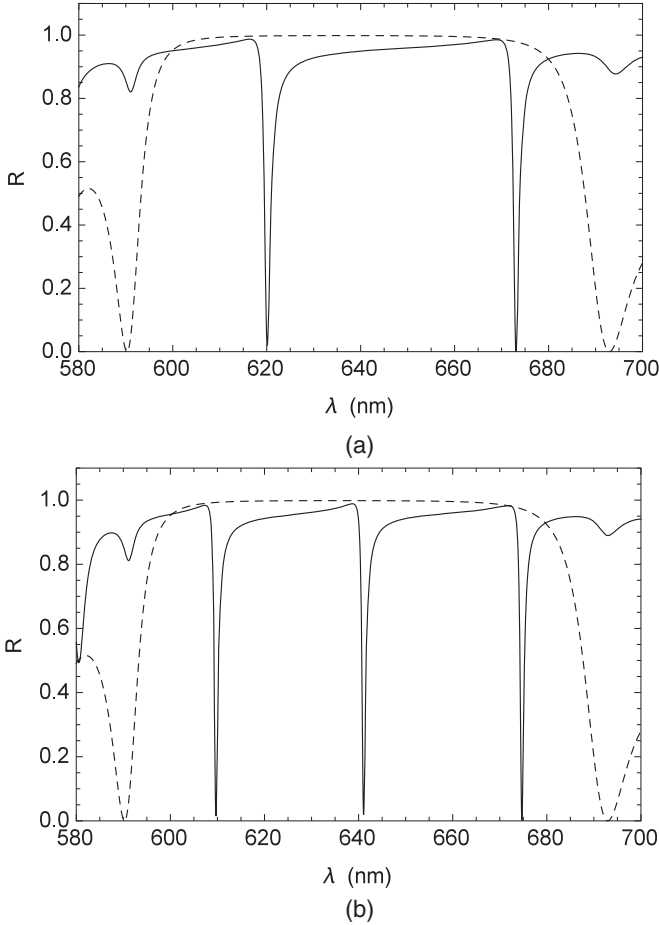
FIG. 7. Reflection dips in the spectral region of the CLC band gap for different thicknesses of the DIML: (a) $d = 4.6p$; (b) $d = 8.3p$. CLC pitch $p = 400$ nm, thickness of the Ag film $l = 36$ nm.

be the difference between the phase incursions of forward and backward waves at wavelength λ_1 caused by the DIML. Denote by φ_0 its value, which corresponds to the wave's interference maximum associated with the OTSs at the wavelength λ_1, i.e., $2\pi \frac{2d}{\lambda_1} \bar{n} = \varphi_0$. However, the interference maximum (and therefore OTS) will also be at wavelength λ_2, when the phases $2\pi \frac{2d}{\lambda_1} \bar{n}$ and $2\pi \frac{2d}{\lambda_2} \bar{n}$ differ by $2\pi m$. Assuming $m = 1$, we obtain the equality $\frac{1}{\lambda_1} - \frac{1}{\lambda_2} = \frac{1}{2\bar{n}d}$. The band gap of the CLC with pitch p is within wavelength range $[n_o p, \ n_e p]$ [36]. Therefore, OTS at wavelengths λ_1 and λ_2 can be simultaneously in the CLC band gap, when $n_o p < \lambda_1, \lambda_2 \ < n_e p$, which implies, as can be seen, the limitation on the smallness of the DIML thickness d. The appearance of the third and other OTSs can be explained in a similar way, by setting an integer $m = 2, \ 3, \ ....$ Simple calculations show that the appearance of s OTS in the CLC band gap requires the DIML thickness be

$d > (s-1) \frac{n_0 n_e}{(n_e - n_0) \bar{n}} \frac{p}{2}$. This estimate is in good agreement with the results of numerical simulations shown, in particular, in Fig. 7.

IV. CONCLUSIONS

The reflection spectrum of a system consisting of a metal film and two adjacent sequentially located CLCs with opposite helix twist is theoretically studied in the field of an incident linearly polarized light wave. The system contains a dielectric index-matching layer (DIML) affecting the phase incursion of the waves between the metal film and the CLC. The CLC layer thickness is large enough to neglect the passage of waves with the same circular polarization as the CLC helical twist. In numerical calculations, Ag is used as a metal film.

A reflection dip in the spectral region of the CLC band gap is obtained, associated with the appearance of OTSs at the interface of the metal film and the CLC layer. The OTS arises due to the interference at the interface of direct and backward waves repeatedly reflected from the CLC and the Ag film. The DIML located between these reflective layers affects the phase of the waves and, consequently, the wavelength and magnitude of the localized light packet corresponding to OTS. The dependence of the spectral position and the magnitude of the OTS dip on DIML thickness, CLC pitch, refractive indices, and Ag film thickness is obtained. The strong influence of the DIML thickness on the OTS wavelength is established, which makes it possible to obtain the OTS dip in the reflection spectrum at the required wavelength within the CLC band gap. It is shown that multiple OTSs can appear in the CLC band gap with an increase of the DIML thickness.

Although the analysis presented in this paper is confined to normally incident plane waves, obliquely incident plane waves may be better in some circumstances for OTS excitation. There is an optimal angle of incidence that provides the maximum reflection dip and its position in the CLC band gap. It depends, in particular, on the polarization of the incident light, as has been shown for the metal-dielectric-Bragg mirror system [5], but it is problematic to predict such changes from general considerations when CLCs are present. Also, the presented analysis applies to a normally incident beam with a cross-sectional diameter much larger (>10 times) than the free-space wavelength. If, however, that cross-sectional diameter of the incident beam is smaller, beam reflection will be affected by the cross-sectional diameter and the field profile of the incident beam [47–49]. The effects of the beam parameters on OTS excitation require investigation.

[1] A. V. Kavokin, I. A. Shelykh, and G. Malpuech, Lossless interface modes at the boundary between two periodic dielectric structures, Phys. Rev. B **72**, 233102 (2005).

[2] A. P. Vinogradov, A. V. Dorofeenko, S. G. Erokhin, M. Inoue, A. A. Lisyansky, A. M. Merzlikin, and A. B. Granovsky,

Surface state peculiarities in one-dimensional photonic crystal interfaces, Phys. Rev. B **74**, 045128 (2006).

[3] T. Goto, A. V. Dorofeenko, A. M. Merzlikin, A. V. Baryshev, A. P. Vinogradov, M. Inoue, A. A. Lisyanskii, and A. B. Granovsky, Optical Tamm States in One-Dimensional

Magnetophotonic Structures, Phys. Rev. Lett. **101**, 113902 (2008).

[4] A. Gaspar-Armenta and F. Villa, Photonic surface-wave excitation: Photonic crystal-metal interface, J. Opt. Soc. Am. B **20**, 2349 (2003).

[5] M. Kaliteevski, I. Iorsh, S. Brand, R. A. Abram, J. M. Chamberlain, A. V. Kavokin, and I. A. Shelykh, Tamm plasmon-polaritons: Possible electromagnetic states at the interface of a metal and a dielectric Bragg mirror, Phys. Rev. B **76**, 165415 (2007).

[6] S. Brand, M. A. Kaliteevski, and R. A. Abram, Optical Tamm states above the bulk plasma frequency at a Bragg stack/metal interface, Phys. Rev. B **79**, 085416 (2009).

[7] B. I. Afinogenov *et al.*, Observation of hybrid state of Tamm and surface plasmon-polaritons in one-dimensional photonic crystals, Appl. Phys. Lett. **103**, 061112 (2013).

[8] M. E. Sasin, R. P. Seisyan, M. A. Kalitteevski, S. Brand, R. A. Abram, J. M. Chamberlain, A. Yu. Egorov, A. P. Vasil'ev, V. S. Mikhrin, and A. V. Kavokin, Tamm plasmon polaritons: Slow and spatially compact light, Appl. Phys. Lett. **92**, 251112 (2008).

[9] S. Y. Vetrov, R. G. Bikbaev, and I. V. Timofeev, Optical Tamm states at the interface between a photonic crystal and a nanocomposite with resonance dispersion, J. Exp. Theor. Phys. **117**, 988 (2013).

[10] V. Yu. Reshetnyak, I. P. Pinkevych, T. J. Bunning, and D. R. Evans, Influence of rugate filters on the spectral manifestation of Tamm plasmon-polaritons, Materials **14**, 1282 (2021).

[11] A. M. Vyunishev, R. G. Bikbaev, S. E. Svyakhovskiy, I. V. Timofeev, P. S. Pankin, S. A. Evlashin, S. A. Vetrov, S. A. Myslivets, and V. G. Arkhipkin, Broadband Tamm plasmon polariton, J. Opt. Soc. Am. B **36**, 2299 (2019).

[12] J. A. Polo, T. G. Mackay, and A. Lakhtakia, in *Electromagnetic Surface Waves: A Modern Perspective* (Elsevier, Waltham, MA, 2013), Chap. 2.

[13] W. L. Zhang, F. Wang, Y. J. Rao, and Y. Jiang, Novel sensing concept based on optical Tamm plasmon, Opt. Express **22**, 14524 (2014).

[14] B. Auguié, M. C. Fuertes, P. C. Angelomé, N. L. Abdala, G. J. A. A. Soler Illia, and A. Fainstein, Tamm plasmon resonance in mesoporous multilayers: Toward a sensing application, ACS Photonics **1**, 775 (2014).

[15] A. V. Baryshev and A. M. Merzlikin, Approach to visualization of and optical sensing by Bloch surface waves in noble or base metal-based plasmonic photonic crystal slabs, Appl. Opt. **53**, 3142 (2014).

[16] S. Kumar, P. S. Maji, and R. Das, Tamm-plasmon resonance based temperature sensor in a Ta_2O_5/SiO_2 based distributed Bragg reflector, Sens. Actuators A **260**, 10 (2017).

[17] P. S. Maji, M. K. Shukla, and R. Das, Blood component detection based on miniaturized self-referenced hybrid Tamm-plasmon-polariton sensor, Sens. Actuators B **255**, 729 (2018).

[18] C. Symonds, A. Lemaître, P. Senellart, M. H. Jomaa, S. Aberra Guebrou, E. Homeyer, G. Brucoli, and J. Bellessa, Lasing in a hybrid GaAs/silver Tamm structure, Appl. Phys. Lett. **100**, 121122 (2012).

[19] R. Brückner, A. A. Zakhidov, R. Scholz, M. Sudzius, S. I. Hintschich, H. Fröb, V. G. Lyssenko, and K. Leo, Phase-locked coherent modes in a patterned metal–organic microcavity, Nat. Photonics **6**, 322 (2012).

[20] C. Symonds, G. Lheureux, J. P. Hugonin, J. J. Greffet, J. Laverdant, G. Brucoli, A. Lemaitre, P. Senellart, and J. Bellessa, Confined Tamm plasmon lasers, Nano Lett. **13**, 3179 (2013).

[21] W. L. Zhang and S. F. Yu, Bistable switching usingan optical Tamm cavity with a Kerr medium, Opt. Commun. **283**, 2622 (2010).

[22] H. Cheng, C. Kuo, Y. Hung, K. Chen, and S. Jeng, Liquid-Crystal Active Tamm-Plasmon Devices, Phys. Rev. Appl. **9**, 064034 (2018).

[23] Y. Gong, X. Liu, H. Lu, I. Wang, and G. Wang, Perfect absorber supported by optical Tamm states in plasmonic waveguide, Opt. Exp. **19**, 18393 (2011).

[24] Z.-Y. Yang, S. Ishii, T. Yokoyama, T. D. Dao, M.-G. Sun, T. Nagao, and K.-P. Chen, Tamm plasmon selective thermal emitters, Opt. Lett. **41**, 4453 (2016).

[25] Z.-Y. Yang, S. Ishii, T. Yokoyama, T. D. Dao, M.-G. Sun, P. S. Pankin, I. V. Timofeev, T. Nagao, and K.-P. Chen, Narrowband wavelength selective thermal emitters by confined Tamm plasmon polaritons, ACS Photonics **4**, 2212 (2017).

[26] O. Gazzano, S. M. Vasconcellos, K. Gauthron, C. Symonds, P. Voisin, J. Bellessa, A. Lemaître, and P. Senellart, Single photon source using confined Tamm plasmon modes, Appl. Phys. Lett. **100**, 232111 (2012).

[27] M. I. Dyakonov, New type of electromagnetic wave propagating at an interface, Sov. Phys. JETP **67**, 714 (1988).

[28] T. G. Mackay, C. Zhou, and A. Lakhtakia, Dyakonov–Voigt surface waves, Proc. R. Soc. London, Ser. A **475**, 20190317 (2019).

[29] Y. Li, J. Sun, Y. Wen, and J. Zhou, Controllable Selective Coupling of Dyakonov Surface Waves at a Liquid-Crystal-Based Interface, Phys. Rev. Appl. **13**, 024024 (2020).

[30] V. Yu. Reshetnyak, V. I. Zadorozhnii, I. P. Pinkevych, and D. R. Evans, Liquid crystal control of the plasmon resonances at terahertz frequencies in graphene microribbon gratings, Phys. Rev. E **96**, 022703 (2017).

[31] V. Yu. Reshetnyak, V. I. Zadorozhnii, I. P. Pinkevych, T. J. Bunning, and D. R. Evans, Surface plasmon absorption in MoS_2 and graphene$-MoS_2$ micro-gratings and the impact of a liquid crystal substrate, AIP Adv. **8**, 045024 (2018).

[32] O. Takayama, L. Crasovan, D. Artigas, and L. Torner, Observation of Dyakonov Surface Waves, Phys. Rev. Lett. **102**, 043903 (2009).

[33] V. Yu. Reshetnyak, T. J. Bunning, and D. R. Evans, Using liquid crystals to control surface plasmons, Liq. Cryst. **45**, 2010 (2018).

[34] O. Buchnev, A. Belosludtsev, V. Reshetnyak, D. R. Evans, and V. A. Fedotov, Observing and controlling a Tamm plasmon at the interface with a metasurface, Nanophotonics **9**, 897 (2020).

[35] V. Yu. Reshetnyak, V. I. Zadorozhnii, I. P. Pinkevych, T. J. Bunning, and D. R. Evans, Modelling the surface plasmon spectra of an ITO nanoribbon grating adjacent to a liquid crystal layer, Materials **13**, 1523 (2020).

[36] P. G. de Gennes and J. Prost, in *The Physics of Liquid Crystals* (Clarendon, Oxford, 1993), Chap. 6.

[37] S. Y. Vetrov, M. V. Pyatnov, and I. V. Timofeev, Spectral and polarization properties of a 'cholesteric liquid crystal-phase film-metal' structure, J. Opt. **18**, 015103 (2016).

[38] M. V. Pyatnov, S. Ya. Vetrov, and I. V. Timofeev, Localised optical states in a structure formed by two oppositely handed cholesteric liquid crystal layers and a metal, Liq. Cryst. **44**, 674 (2017).

[39] H. Zhou, G. Yang, K. Wang, H. Long, and P. Lu, Multiple optical Tamm states at a metal-dielectric mirror interface, Opt. Lett. **35**, 4112 (2010).

[40] Y. Fei, Y. Liu, D. Dong, K. Gao, S. Ren, and Y. Fan, Multiple adjustable optical Tamm states in one-dimensional photonic quasicrystals with predesigned band gaps, Opt. Exp. **26**, 34872 (2018).

[41] M. Adams, B. Cemlyn, I. Henning, M. Parker, E. Harbord, and R. Oulton, Model for confined Tamm plasmon devices, J. Opt. Soc. Am. A **36**, 125 (2019).

[42] A. Lakhtakia and I. J. Hodgkinson, Spectral response of dielectric thin-film helicoidal bianisotropic medium bilayer, Opt. Commun. **167**, 191 (1999).

[43] J. Adams, W. Haas, and J. Dailey, Cholesteric films as optical filters, J. Appl. Phys. **42**, 4096 (1971).

[44] D.-K. Yang and S.-T. Wu, in *Fundamentals of Liquid Crystal Devices*, 2nd ed. (John Wiley & Sons, New York, 2015), Chap. 2.

[45] V. Belyakov, in *Diffraction Optics of Complex-Structured Periodic Media* (Springer, Cham, 2019), Chap. 1.

[46] A. D. Rakić, A. B. Djurišic, J. M. Elazar, and M. L. Majewski, Optical properties of metallic films for vertical-cavity optoelectronic devices, Appl. Opt. **37**, 5271 (1998).

[47] F. Wang and A. Lakhtakia, Lateral shifts of optical beams on reflection by slanted chiral sculptured thin films, Opt. Commun. **235**, 107 (2004).

[48] X. Guo, X. Liu, W. Zhu, M. Gao, W. Long, J. Yu, H. Zheng, H. Guan, Y. Luo, H. Lu, J. Zhang, and Z. Chen, Surface plasmon resonance enhanced Goos–Hänchen and Imbert–Fedorov shifts of Laguerre–Gaussian beams, Opt. Commun. **445**, 5 (2019).

[49] S. Shirin, A. Madani, and S. R. Entezar, Tunable lateral shift of the reflected optical beams from a nanocomposite structurally chiral medium, Opt. Mater. **107**, 110026 (2020).